The Seismic Record
A journal of the Seismological Society of America

Stress Drop Variations of Induced Earthquakes near the Dallas–Fort Worth Airport, Texas

Seong Ju Jeong[*1,2], Brian W. Stump[1], and Heather R. DeShon[1]

Abstract

We estimate stress drops for injection-induced earthquakes near the Dallas–Fort Worth Airport in the Fort Worth basin (FWB), Texas, to investigate source properties in response to fluid injection. The stress drops for the Airport sequence show three unique characteristics compared to those estimated for other earthquake sequences in the FWB: (1) stress drops have lower mean and median values; (2) stress drops increase with moment magnitude; and (3) stress drops increase in size over the first 1.5 km in radial distance from the injection point. The low stress drop Airport events occurred shortly after the initiation of injection near a fault within hundreds of meters of the well. Pore pressure perturbations in the Airport area are 1 order of magnitude lower than those from the other sequences, suggesting that absolute pore pressure changes may not be the main factors of stress drop variations. We suggest that the low stress drop events may be related to transition from aseismic slip to seismic rupture previously observed in laboratory and field experiments.

Cite this article as Jeong, S. J., Stump, B. W., and DeShon, H. R. (2022). Stress Drop Variations of Induced Earthquakes near the Dallas–Fort Worth Airport, Texas, *The Seismic Record*. **2**(**2**), 68–77, doi: 10.1785/0320220003.

Supplemental Material

Introduction

Stress drop is a seismic source parameter defined as the difference between the shear stress on a fault before and after earthquake slip. It is a kinematic representation of rupture energy that includes both fault size and the amount of slip. As a result, stress drop is an estimate of average slip per unit fault dimension. For the same fault area, increased slip yields higher stress drop. It is used to quantify differences in slip behavior associated with geology, in situ stress conditions, and fault characteristics. This source representation contributes to estimates of seismic hazard, as it captures the amplitude and frequency content of radiated seismic energy and can add to source type identification (e.g., Chen and Abercrombie, 2020).

Stress drop estimates often denote spatial and temporal changes in natural earthquakes associated with fluid pressure perturbation (e.g., temporal changes [1–3 MPa] for aftershocks from the 2011 Tohoku–Oki earthquake, Yoshida *et al.*, 2017). Similarly, studies of induced earthquakes associated with waste fluid injection indicate that fluid injection can influence stress drop, but there is no consensus on a single quantitative relationship. Yu *et al.* (2020) estimate lower stress drops (0.1–1 MPa) for events in the Montney oil and gas production area that occur within 1 km of a hydraulic fracturing well compared to those associated with earthquakes at further distances (1–10 MPa). Staszek *et al.* (2017) state that stress drop changes of earthquakes in the Geysers geothermal field are inversely related to the injection rate and find no relationship with distance from the injector. Injection-induced earthquakes in Oklahoma and Kansas also produce low stress drop estimates with variation as a function of magnitude but no correlation with distance (Sumy *et al.*, 2017; Trugman *et al.*, 2017).

Here, we estimate stress drops using *S* waves in a data-driven spectral inversion for well-recorded induced earthquakes during the Dallas–Fort Worth (DFW) Airport sequence, which produced unique characteristics relative to other earthquake sequences in the Fort Worth basin (FWB). The DFW Airport

1. Department of Earth Sciences, Southern Methodist University, Dallas, Texas, U.S.A.; 2. Now at Department of Earth Sciences, University of Toronto, Toronto, Ontario, Canada

*Corresponding author: seongju.jeong@utoronto.ca

sequence is estimated to produce earthquakes with a lower mean stress drop of ~1 MPa (Reiter *et al.*, 2012), whereas the other FWB sequences exhibit stress drops consistent with values expected for tectonic events (~5 MPa) (Justinic *et al.*, 2013; Jeong *et al.*, 2020, 2021). Ogwari *et al.* (2018) estimated a higher *b*-value 1.43 for the Airport earthquakes from October to December 2008, compared to lower *b*-values of 0.67–1.01 suggested for the other FWB sequences (Justinic *et al.*, 2013; Quinones *et al.*, 2019). Finally, the Airport sequence is the only one in the FWB that produced earthquake locations that migrated away from a single-source injection well with time (Ogwari *et al.*, 2018). Here, we compute and compare the Airport stress drops to the broader FWB stress drop catalog (Jeong *et al.*, 2020, 2021) using the same estimation methodology. For the Airport sequence, we find stress drop variations as a function of magnitude and distance that increase over the first 1.5 km from the nearest injector, and suggest that these variations may reflect a transition from aseismic to seismic slip as the earthquakes migrate away from the injection source.

Seismicity of the DFW Airport in the FWB, Texas

The FWB has experienced little to no significant seismic deformation over the past 300 Ma (Magnani *et al.*, 2017), in contrast to the seismic activity from 2008 to 2020 when there were over 30 magnitude 3 and above earthquakes and 114 that were felt (e.g., U.S. Geological Survey [USGS] catalog, last accessed March 2022). The FWB earthquakes have been linked to waste fluid injection associated with unconventional oil and gas extraction and wastewater disposal (Ogwari *et al.*, 2018; Quinones *et al.*, 2019). Most of the FWB seismicity occurs on northeast–southwest-trending basement-rooted faults that are optimally oriented for failure within the regional stress field (e.g., Horne *et al.*, 2020; Fig. 1).

FWB seismicity was recorded by a series of seismic networks deployed since 2008 (DeShon *et al.*, 2018). The five best-studied earthquake sequences include: (1) DFW Airport (Frohlich *et al.*, 2011); (2) Cleburne (Justinic *et al.*, 2013); (3) Azle-Reno (Hornbach *et al.*, 2015); (4) Irving-Dallas (Quinones *et al.*, 2018); and (5) Venus (Scales *et al.*, 2017; Figs. 1, 2). The Airport sequence, the focus here, generated 10 events large enough to be reported by the USGS, with magnitudes from 2.5 to 3.0, beginning in October 2008. Subsequently, 11 events with local magnitude from 1.7 to 2.3 were well recorded by a local seismic network installed and operated by Southern Methodist University (SMU) from 9 November 2008 to 2 January 2009. Local recordings from these 11 events are used to estimate Airport stress drops. The hypocenters are within 1 km of an injection well located at the south end of the Airport, whereas the subsequent earthquake locations traced a ~1 km linear feature that coincided with a mapped fault (Fig. 2). Fluid injection began seven weeks before the earthquakes (September 2008), with injection subsequently shut down in August 2009 (Fig. S1, available in the supplemental material to this article). After removal of the SMU local network, the USGS reported an additional 15 events from 16 May 2009 to 14 September 2017. A total 36 events (25 from USGS and 11 from SMU) were observed in the Airport area with significant magnitudes (>1.7). From October 2008 to August 2015, 412 earthquakes, including smaller magnitudes, were identified in the Ogwari *et al.* (2018) using a template approach. The template-matched Airport events cannot be included in this study, as they did not have seismic signals with adequate bandwidth to make stress drop estimates. Unlike the Airport earthquakes, the other FWB sequences occur over longer time spans (~2–5 yr), and greater distances between initial fluid injection at nearby (<10 km) wells and the onset seismicity (Fig. S1).

Data and Methods

Seismic data from the Airport events were recorded at distances from 2 to 25 km with good azimuthal coverage and sampled at 100 or 200 samples per second (DeShon *et al.*, 2018, Fig. S2). *S*-wave spectral estimation follows the procedure outlined in Jeong *et al.* (2020) and used for the other FWB earthquakes, with spectra from 1 to 25 Hz. Seismograms that were used to produce the spectral estimates had signal-to-noise ratios of ≥3 in each of five frequency bands (1–5, 5–10, 10–15, 15–20, and 20–25 Hz).

Individual earthquake spectra need to be separated into a number of effects to estimate the stress drops for the Airport earthquakes. The generalized inversion technique (GIT) provides a methodology to separate source spectra, path attenuation characteristics, and site response based on Fourier amplitude spectra from *S* waves. In the frequency domain, the logarithm of observed spectra represents the linear contribution of the three primary factors, including the source, path, and site effects. This linear representation is solved using least squares in two steps. First, we utilized path terms from Jeong *et al.* (2020), which quantified propagation characteristics for the FWB. After correcting for the FWB path attenuation, a GIT inversion was performed using the 54 recordings from the 11

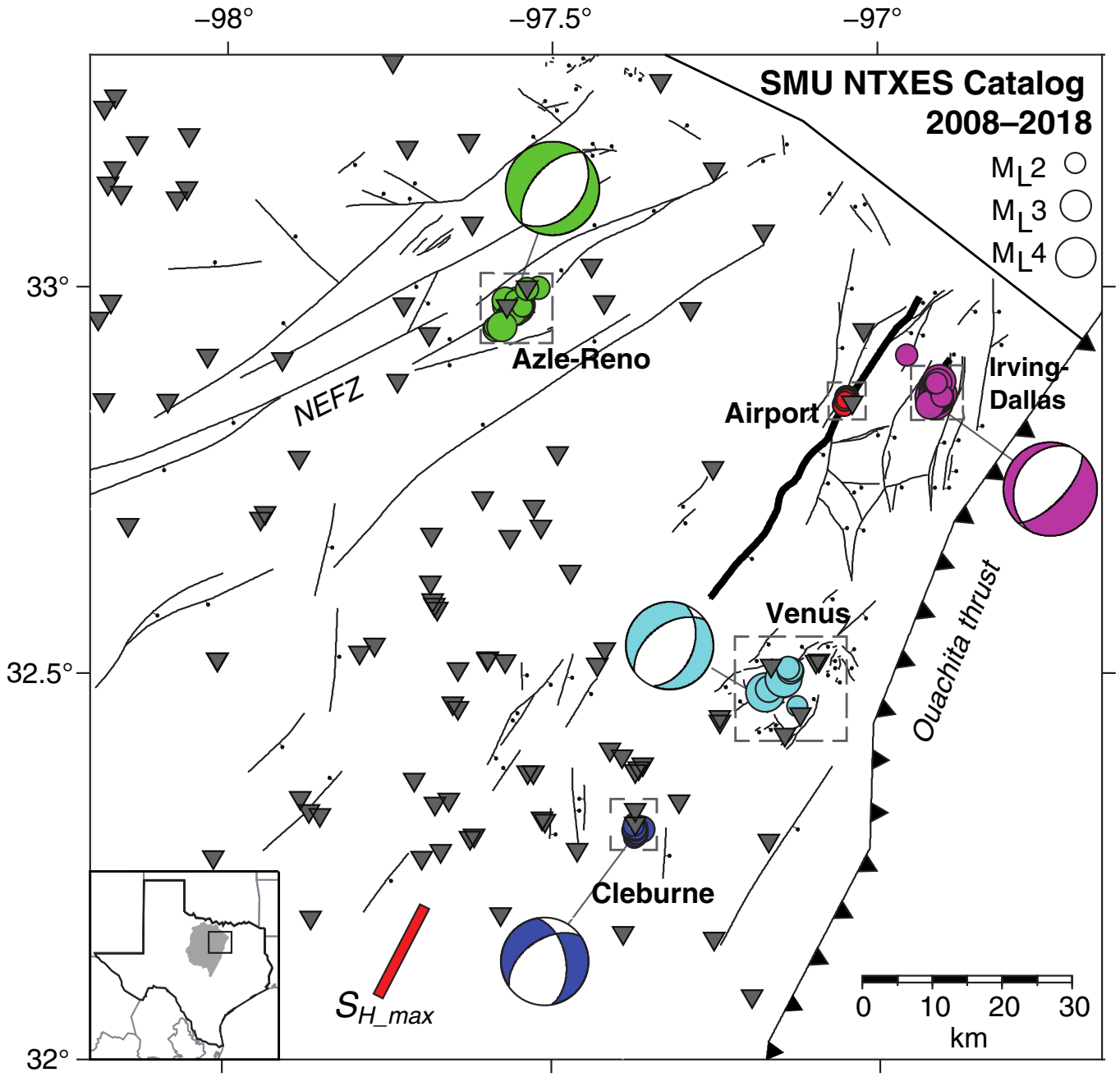

Figure 1. The events in the Southern Methodist University (SMU) North Texas earthquake catalog are mapped, including events near the Dallas–Fort Worth (DFW) Airport (red circle), Cleburne (blue), Azle-Reno (green), Irving-Dallas (purple), and Venus (cyan) in the Fort Worth basin (FWB), Texas (modified from Quinones *et al.*, 2019). Boxes indicate the boundaries used in Figure 2. Focal mechanisms are from Justinic *et al.* (2013) and Quinones *et al.* (2018). Regional faults (solid black lines) with the downthrown hanging-wall block (black dots) are from Horne *et al.* (2020) and plotted at the top of the crystalline basement. The bold line indicates the mapped seismogenic fault for the DFW Airport sequence. Waste fluid injection wells (gray inverted triangles) and the maximum horizontal stress (S_{H_max}) orientation from Lund Snee and Zoback (2016) (red bar) are also shown. Inset shows Texas and the Barnett Shale distribution (gas production layer) in the FWB (gray).

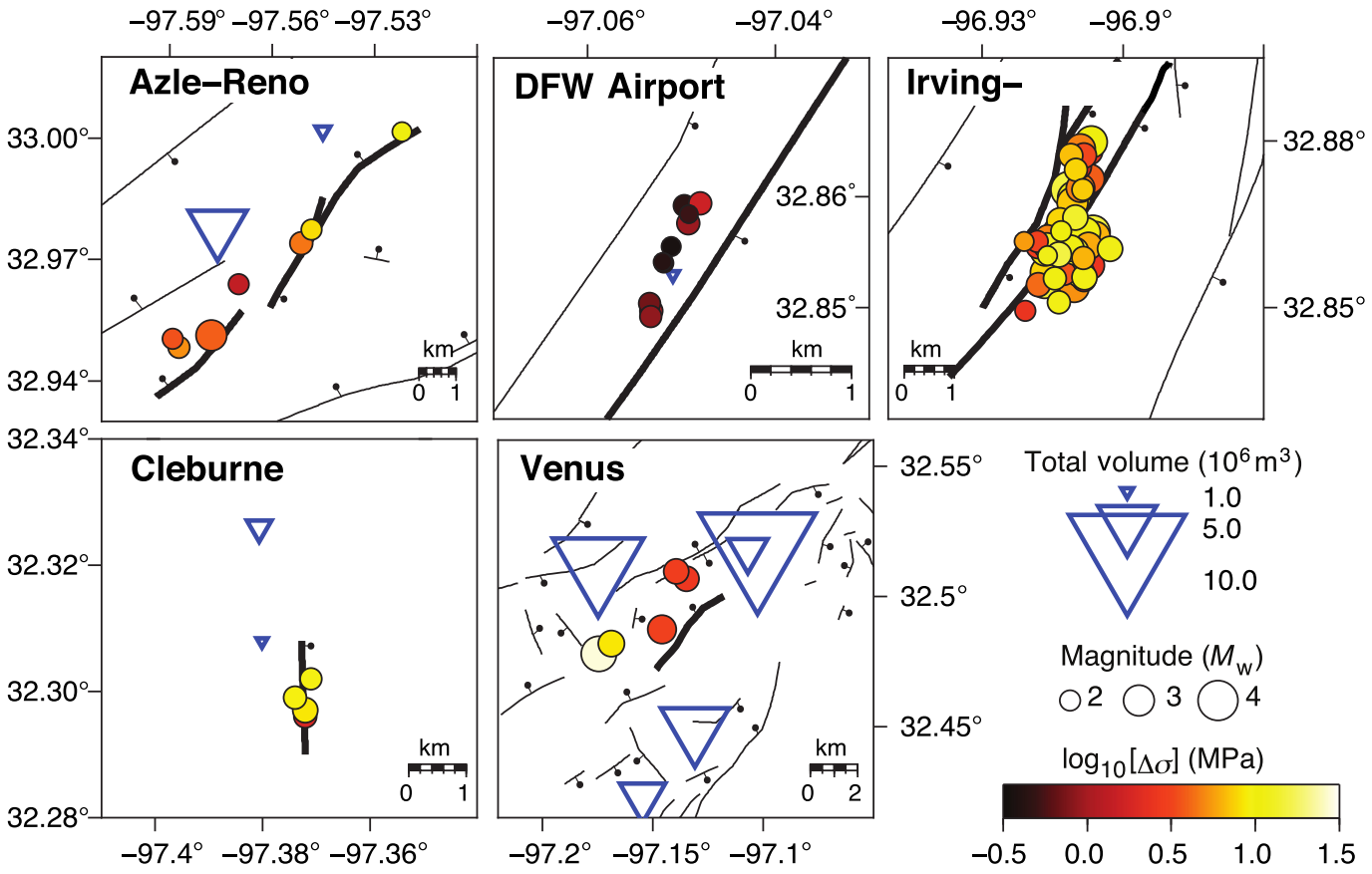

Figure 2. The earthquake locations used in the analysis from the five named FWB earthquake sequences that include Azle-Reno, DFW Airport, Irving-Dallas, Cleburne, and Venus. Events are color coded by stress drop estimates using generalized inversion technique (GIT) (see Data and Methods section for details). Injection wells are scaled by total volume from 2005 to 2018 (blue inverted triangles). Seismogenic faults are highlighted as bold lines with black dots indicating the downthrown hanging-wall block for each fault (Horne *et al.*, 2020). Sequence locations are shown in Figure 1.

well-recorded Airport earthquakes taking station AFMOM as the reference site, to avoid a trade-off between source and the site contributions. The reference station AFMOM was chosen based on the site characterization that produces GIT H (horizontal) estimates in good agreement with horizontal-to-vertical spectral ratios (HVSRs) and GIT V (vertical) with little or no variation as a function of frequency (Jeong *et al.*, 2020). The estimate of GIT V is constrained, so the average value for all the sites is one under the assumption that there should be small site amplifications on vertical components. GIT H for AFMOM is estimated using the site correction method described in Jeong *et al.* (2020).

The 11 Airport earthquake locations and magnitudes were estimated in three previous studies (Frohlich *et al.*, 2011; Reiter *et al.*, 2012; Ogwari *et al.*, 2018). Locations in these studies are similar, with the most significant difference being a 0.45 ± 0.24 km depth difference between the Frohlich and Reiter catalogs (Fig. 3a). To determine which of the three catalog magnitudes to use as a reference, we estimated site effects for AFMOM using the three different local magnitudes (Fig. 3b) and compared them to estimates of HVSR. The Frohlich *et al.* (2011) magnitudes produced the most consistent estimates of GIT H site amplification within the standard deviation of HVSR. Site amplification functions estimated using the magnitudes of Reiter *et al.* (2012) are slightly underestimated (i.e., larger moments), whereas those using magnitudes from Ogwari *et al.* (2018) overestimate the site effect (i.e., smaller moments). We, therefore, use the Frohlich *et al.* (2011) catalog as our reference. The GIT site effects for the Airport stations are included in the supplemental material (Fig. S3).

Based on the source spectra extracted using GIT for the earthquakes in the DFW Airport sequence, we estimate seismic moment, corner frequency, and stress drop based on a Brune

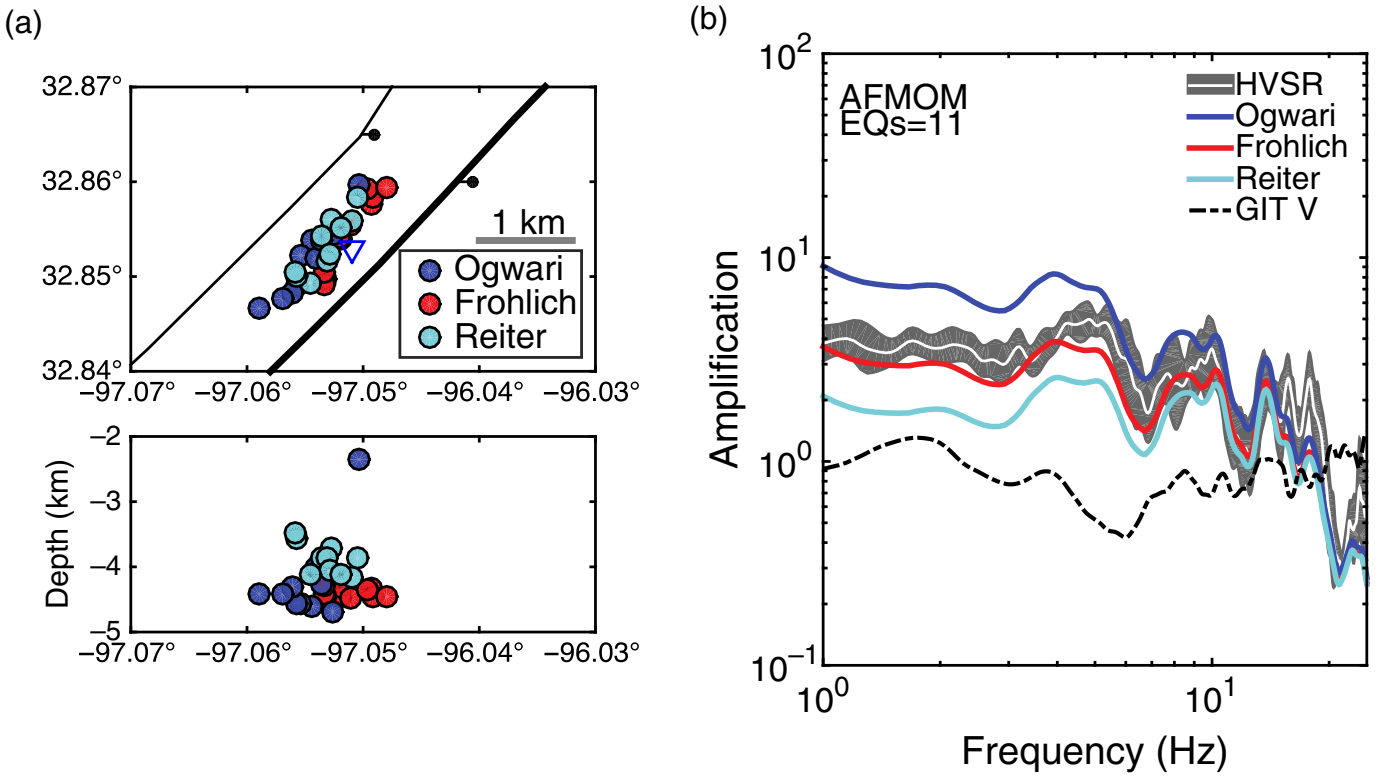

Figure 3. DFW Airport event catalog selection criteria. (a) Map showing epicentral locations from the three different catalogs. Black lines are the location of faults from Horne *et al.* (2020). The seismogenic fault is highlighted as the thicker line. Black dots indicate the downthrown hanging-wall block for each fault. The blue inverted triangle represents the injection well. The cross-section view is below. (b) Site response functions for station AFMOM from the DFW Airport sequence. The GIT site effects for the horizontal components estimated using magnitudes from multiple publications are illustrated as continuous lines in different colors. The vertical site response (GIT V; dashed line), horizontal-to-vertical spectral ratio (HVSR; white lines) with the mean ± one standard deviation (gray shaded area), the station name, and the number of earthquakes (EQs) are displayed.

source model (Brune, 1970), $S(f) = \Omega_0/(1 + [f/f_c]^2)$, in which Ω_0 is the low-frequency amplitude, f_c is the corner frequency, and f is the frequency. The details of the inversion process for source parameters are included in Jeong *et al.* (2020, 2021).

As a check on the methodology, stress drop estimates are also made using empirical Green's functions (EGFs). This comparison allows assessment of possible attenuation differences between the Airport fault zone and other fault zones in the FWB. Here, we follow the EGF method documented in Jeong *et al.* (2021). The GIT method is considered the primary method for comparison, as stress drops from the other FWB sequences were estimated using GIT and compared to estimates using the EGF method for only 14 events (Jeong *et al.*, 2021).

Results

Stress drops for the DFW Airport sequence using GIT are compared to estimates for the other FWB earthquakes in terms of spatiotemporal distributions and moment magnitudes (Figs. 2, 4). Because stress drops are model dependent, we produce consistent model estimates for all five sequences. Stress drops for the Cleburne, Azle–Reno, Irving–Dallas, and Venus sequences are invariant to the time and location of events relative to the nearest injectors (Fig. 4). The one sequence that differs from these others is the DFW Airport sequence with lower stress drops. DFW Airport stress drops have a mean of 0.41 MPa and a median value of 0.42 MPa, compared to all the other FWB events with a mean of 2.87 MPa and a median of 3.06 MPa (Fig. 4e). Details of the stress drop estimates are documented in Dataset D1 in the supplemental material.

Stress drop differences between the DFW Airport and other sequences are approximately an order of magnitude in terms of both mean and median values—an indication that the Airport

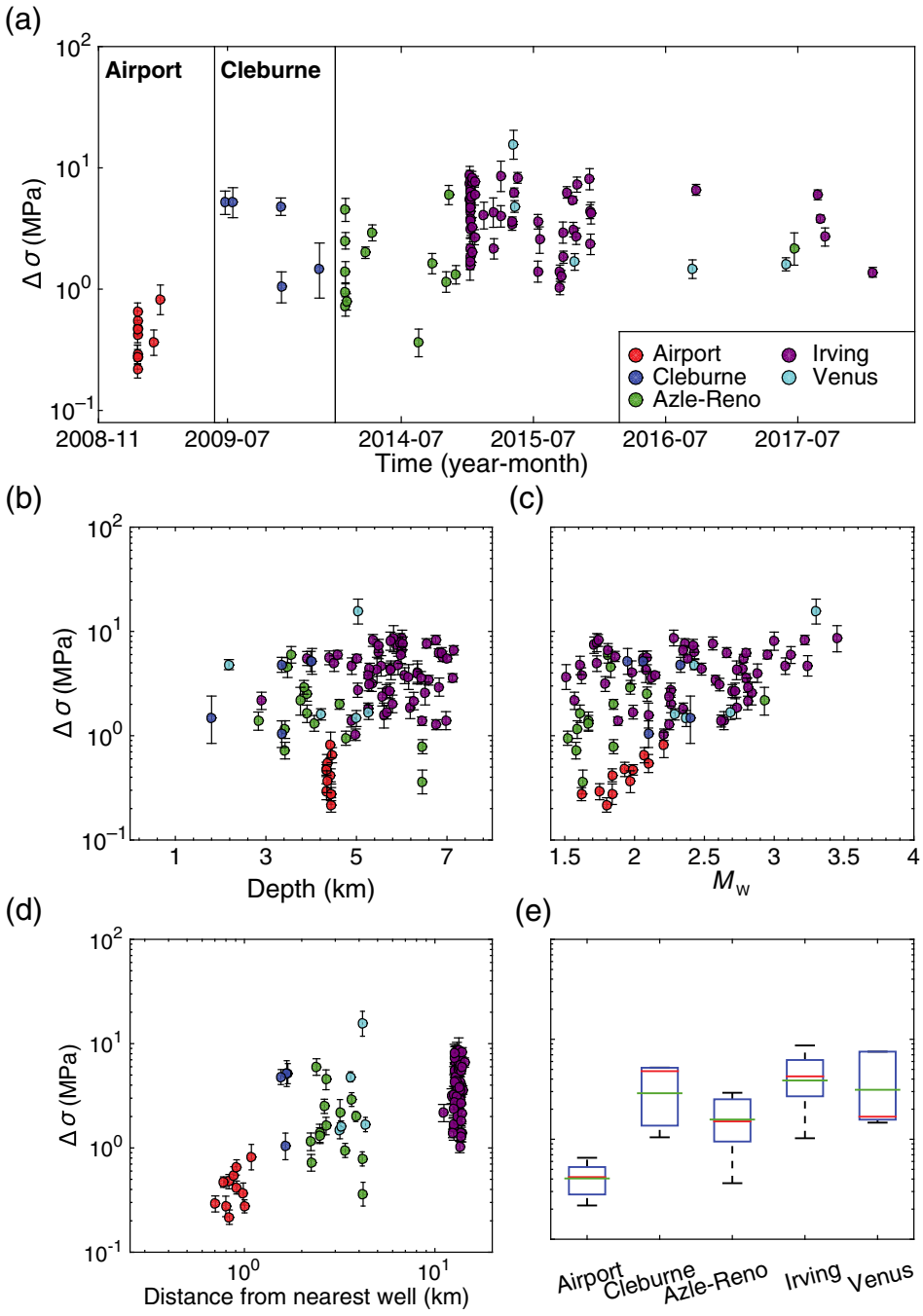

Figure 4. Stress drop estimates are plotted against (a) time, (b) event depth, (c) moment magnitude M_w, (d) distances from the nearest injection points, and (e) box plots. (a–d) Error bars represent the 95% confidence intervals for the stress drop estimates. Colors indicate individual sequences following Figure 1 and are described in the legend in (a). In (a), note the time breaks after both the Airport and Cleburne sequences. (c,d) The Airport earthquakes display an increase in stress drop with magnitude and range, whereas stress drops from the other sequences do not correlate with moment magnitude or distance. Note that the Irving–Dallas sequence locates at >10 km from the nearest well in (d). In (e), each box plot includes the mean (green lines) and median (red lines) values with the 25th and 75th percentiles at the bottom and top boundaries of each blue box, respectively. The whiskers extend to one times the interquartile range. For Cleburne and Venus, stress drops show significant differences between mean and median values due to the small sample sizes. The median values in real numbers are 0.42, 4.80, 1.50, 4.26, and 1.68 MPa for Airport, Cleburne, Azle-Reno, Irving-Dallas, and Venus, respectively. The mean values are 0.41, 2.89, 1.58, 3.87, and 3.13 MPa for each earthquake sequence.

stress drop estimates are significantly lower than those for the other sequences. Comparisons of the time histories of stress drops in the FWB over the last decade do not indicate changes as a function of time, as the subsurface pore fluid pressures evolve with gas development and fluid injection in the basin (Fig. 4a). The depth estimates for the Airport events are similar to those for the other FWB sequences (Fig. 4b).

The stress drops from the Airport events show a positive correlation with magnitude, although the range of magnitudes is limited (M_w 1.6–2.2) and, thus, does not fully support a breakdown in self-similar scaling (Fig. 4c). In addition, the Airport stress drops increase with increasing radial distance from the injector up to 1.5 km (Fig. 4d), consistent with findings in other studies (Chen and Abercrombie, 2020; Yu *et al.*, 2020), although again the sample size in this case is limited. These results indicate that both magnitude and stress drop increase as the Airport earthquakes migrate away from the injector (Fig. S4). The distance to the nearest injector is estimated for each sequence and is calculated from injection points to earthquake hypocenter using the closest injector (Fig. 2), accounting for both earthquake location errors (~300 m) and injection depth uncertainty. Injection takes place over discrete intervals within a well, and, thus, we

assign the average value of the injection interval as the "injection depth" in this study.

Stress drops for other sequences in the FWB are invariant to magnitude (Fig. 4c) and radial distance from the nearest injection point (Fig. 4d). These results indicate that stress drops for events at distances greater than 1.5 km from the injector have higher stress drops consistent with tectonic intraplate earthquakes with values from 1 to 10 MPa (Kanamori and Anderson, 1975).

Discussion

Stress drop estimates for the DFW Airport events are statistically lower than those for other earthquake sequences in the FWB (Fig. 4e). The lower stress drop Airport earthquakes uniquely occur within 1.5 km of the injector and on a high-throw (>200 m) regional fault (Horne *et al.*, 2020) thought to be crossed by or very near to the injector (Ogwari *et al.*, 2018). Stress drops increase with radial distance from the injection depth concurrent with increasing moment magnitudes. We do not find any temporal correlation in these estimates, probably due to the short time period over which the 11 Airport earthquakes in this study occurred (Fig. 4a). The Airport sequence of earthquakes otherwise shares similar characteristics with the rest of the FWB earthquakes. All sequences occur on preexisting normal faults well oriented for failure at or below the sedimentary basement interface producing a series of moderate-to-small events that suggests that the variation in stress drop may not be driven by the tectonic setting (e.g., focal mechanism and directivity effects).

The lower magnitude earthquakes in the Airport sequence may lead to significant trade-offs between attenuation and corner frequency than found for larger earthquakes (Chen and Abercrombie, 2020). To assess this possibility, we apply the EGF method to estimate and compare corner frequencies from the two approaches—GIT and EGF (Fig. 5). EGF source estimates using data from the same earthquakes are found to be similar to the GIT estimates with a mean corner frequency difference of −0.27 Hz, for which EGF method corner frequencies are slightly larger than the GIT estimates (Fig. 5d). Similarly, for 14 larger events from the other FWB sequences, EGF and GIT comparisons (Jeong *et al.*, 2021) also suggest consistent corner frequencies with a small difference of −0.31 Hz (EGF $f_c >$ GITf_c). EGF estimates for the Airport earthquakes also produce stress drops that are dependent on moment magnitude as well as radial distance from the injection point similar to relationships denoted using the GIT stress drops (Fig. S5). Stress drop values using the EGF method are included in Dataset D2 in the supplemental material.

Pore pressure diffusion modeling may provide insight into stress drop variations. Gao *et al.* (2021) estimated pore pressure changes in the FWB based on a 3D hydrogeologic model using extensive geologic constraints, reservoir fluid flow properties, and locations and geometries of fault. Pore pressures are calculated at the location of the sedimentary-basement boundary and provide average pore pressure estimates for active faults at this boundary. The pore pressure change at the initiation of the Airport sequence is small, ∼0.03 MPa (Hennings *et al.*, 2021), due to the short time and space between initiation of fluid disposal and the first earthquakes as well as the moderate volume of the injector. This estimate is 1 order of magnitude smaller than estimates at the start of the other FWB sequences (Hennings *et al.*, 2021). Similarly, Zhai and Shirzaei (2018) estimate coulomb failure stress changes in the FWB using injection data that are 0.005 MPa for the Airport and 0.35–0.4 MPa for Cleburne and Azle–Reno, consistent with the larger injected volumes. These regional modeling studies predict that the absolute pore pressure changes near the Airport injector were low at the initiation of the Airport earthquakes and suggest that the absolute value of pore pressure change may not be the only physical property directly linked to earthquake rupture characteristics like stress drop.

Airport seismicity occurred much closer to the injector and at shorter time lags following the onset of fluid injection than any other FWB sequence (Fig. S6). These characteristics, along with the lower stress drop estimates, are consistent with aseismic slip accompanying events near the injection point, as documented in both field and laboratory experiments (e.g., Guglielmi *et al.*, 2015; Cappa *et al.*, 2019). Guglielmi *et al.* (2015) conducted a large-scale field experiment that quantified changes in fault displacement and fluid pressure following artificial water injection into a preexisting fault in southeastern France. These results suggest that when pore pressure increases, preexisting faults may initially experience aseismic slip rather than typical induced fault slip. During the aseismic period, observed seismicity accounts for only a portion of the total seismic moment release (i.e., lower effective normal stress and stress drop). For events that occurred in this experiment, Huang *et al.* (2019) estimate significantly lower stress drops (0.01 MPa), and suggest that the initial fluid pressure perturbation and aseismic deformation influence the earthquake source properties. The mechanisms of aseismic slip are hypothesized as either (1) a dilatant strengthening created by fracture networks associated with fluid injection or (2) locally

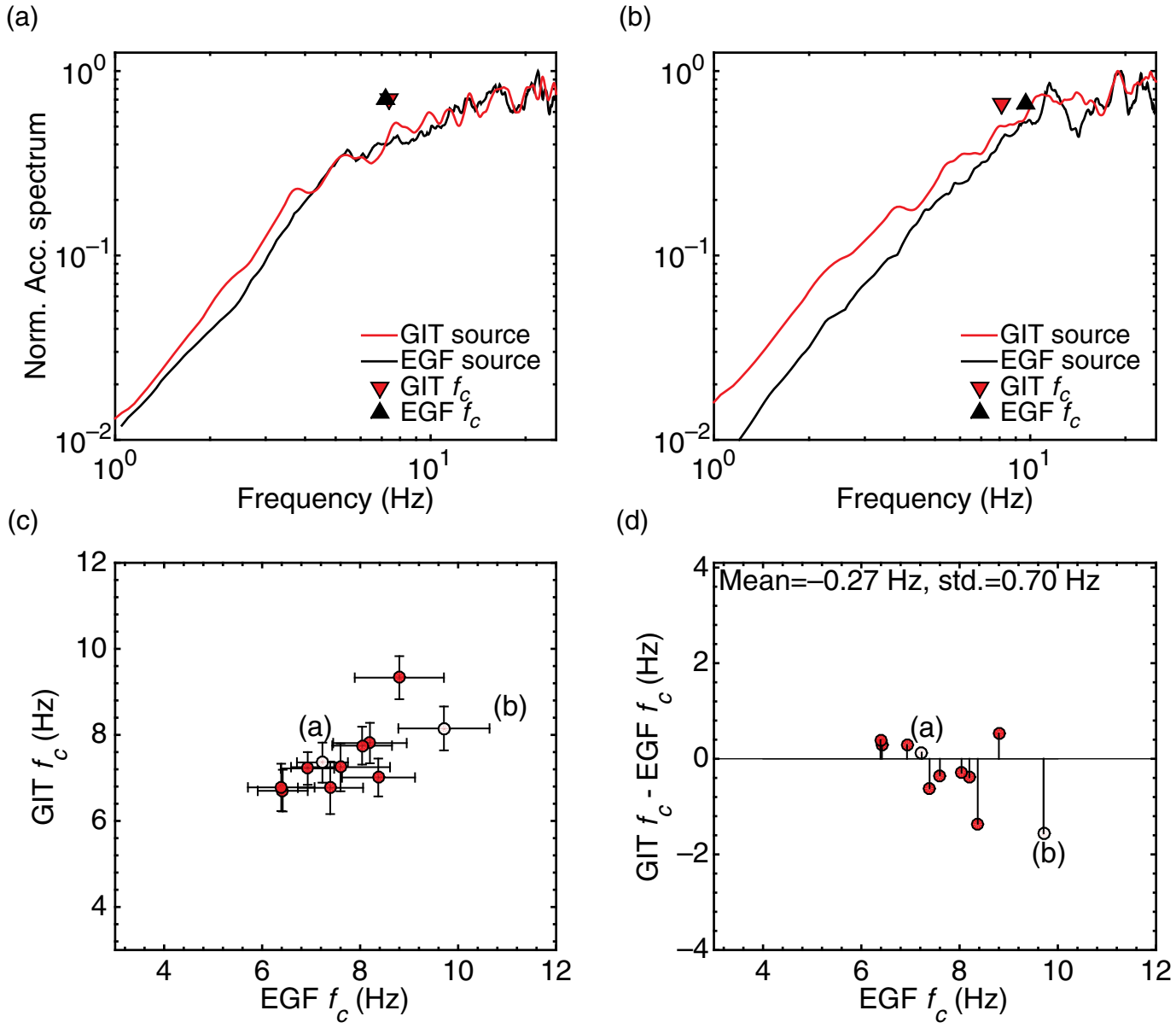

high pore pressure in close proximity to the well resulting in rate-strengthening friction (Guglielmi *et al.*, 2015). In the FWB, where earthquakes are shown to occur on preexisting faults, we would favor the latter interpretation. Even if the absolute pore pressure in DFW Airport area is relatively low, the local zone of high pore pressurization near the injection well may contribute to frictional stability and aseismic motion on the fault plane (Lengliné *et al.*, 2014). However, in this study, we do not have enough data in time and/or space to completely resolve the role of aseismic processes (Fig. S6). The first events in the Airport sequence had larger magnitudes, possibly related to larger seismogenic faults (Figs. 1, 2). In the case of the other

Figure 5. Comparison of (a,b) GIT and empirical Green's function (EGF) source spectra and (c,d) corner frequencies. (a) Normalized spectra for an example event showing similar corner frequency values using the GIT (red) and EGF methods (black), and (b) another example illustrating different corner frequencies estimated using the two approaches. (c) GIT corner frequencies with 95% confidence intervals plotted against EGF corner frequencies with 95% confidence intervals. (d) Residuals between GIT and EGF corner frequencies. The mean and standard deviation of the residuals are noted in the plot. In (c,d), white circles denote example events shown in (a) and (b).

FWB sequences, we may have missed the initial earthquakes with aseismic slip due to a lack of local monitoring that precluded the recording of smaller events.

Conclusions

Anomalously low stress drops are estimated for an earthquake sequence near DFW Airport compared to other earthquakes recorded in the FWB over the last decade. The DFW Airport stress drops increase with both moment magnitude and radial distance from the causative injector out to a distance of 1.5 km. Other earthquake sequences recorded in the FWB occur at distances much greater than 1.5 km from individual injectors and at much longer times following the initiation of fluid injection, and show no spatial or temporal correlations nor magnitude dependence. These events also have significantly higher stress drops consistent with natural intraplate earthquakes. Focal depths and absolute pore pressure changes (or cumulative amount of the injected wastewater) may not be the only controlling factors contributing to stress drop variations. Based on the abrupt onset of seismicity following a moderate volume of fluid injection near a large regional fault, we suggest that transition from aseismic slip to seismic rupture at short time lags and close distance to injection wells observed in laboratory and field experiments may explain the lower stress drops for the DFW Airport events. However, with only 11 Airport events, the complete assessment of stress drop variations associated with magnitude and distance from the injector warrants additional study.

Data and Resources

The temporary network data are available under Federated Digital Seismic Network (FDSN) codes X9 (Southern Methodist University [SMU] 2008–2011, https://doi.org/10.7914/SN/X9_2008). Injection information for saltwater disposal wells is from the Texas Railroad Commission (webapps.rrc.texas.gov/H10/h10PublicMain.do). The figures were made using the Generic Mapping Tools (GMT; Wessel *et al.*, 2013), Inkscape (https://inkscape.org) and MATLAB R2014b (www.mathworks.com/products/matlab). All the websites were last accessed on March 2022. The supplemental material provides supporting Figures S1–S6 and Datasets D1–D2 containing source parameters from the generalized inversion technique (GIT) and empirical Green's function (EGF) method.

Declaration of Competing Interests

The authors acknowledge that there are no conflicts of interest recorded.

Acknowledgments

The study was supported by Department of Earth Sciences at Southern Methodist University (SMU) and through the Texas Seismic Network program at the Bureau of Economic Geology, University of Texas. The seismic instruments were provided by the Incorporated Research Institutions for Seismology (IRIS) through the Program for the Array Seismic Studies of the Continental Lithosphere (PASSCAL) Instrument Center at New Mexico Tech. The authors thank Xiaowei Chen, Editor Keith D. Koper, Associate Editor Ruth Harris, Art McGarr, and another anonymous reviewer for their contributions to improving this article.

References

Brune, J. N. (1970). Tectonic stress and the spectra of seismic shear waves from earthquakes, *J. Geophys. Res.* **75,** 4997–5009, doi: 10.1029/JB075i026p04997.

Cappa, F., M. M. Scuderi, C. Collettini, Y. Guglielmi, and J. P. Avouac (2019). Stabilization of fault slip by fluid injection in the laboratory and in situ, *Sci. Adv.* **5,** eaau4065, doi: 10.1126/sciadv.aau4065.

Chen, X., and R. E. Abercrombie (2020). Improved approach for stress drop estimation and its application to an induced earthquake sequence in Oklahoma, *Geophys. J. Int.* **223,** 233–253, doi: 10.1093/gji/ggaa316.

DeShon, H. R., C. T. Hayward, P. O. Ogwari, L. Quinones, O. Sufri, B. Stump, and M. B. Magnanai (2018). Summary of the North Texas earthquake study seismic networks, 2013-2018, *Seismol. Res. Lett.* **90,** 387–394, doi: 10.1785/0220180269.

Frohlich, C., C. Hayward, B. Stump, and E. Potter (2011). The Dallas–Fort Worth earthquake sequence: October 2008 through May 2009, *Bull. Seismol. Soc. Am.* **101,** 327–340, doi: 10.1785/0120100131.

Gao, R. S., J. P. Nicot, P. H. Hennings, P. La Pointe, K. M. Smye, E. A. Horne, and R. Dommisse (2021). Low pressure build-up with large disposal volumes of oilfield water: A flow model of the Ellenburger Group, Fort Worth Basin, northcentral Texas, *AAPG Bull.* **105,** 2575–2593, doi: 10.1306/03252120159.

Guglielmi, Y., F. Cappa, J. P. Avouac, P. Henry, and D. Elsworth (2015). Seismicity triggered by fluid injection-induced aseismic slip, *Science* **348,** 1224–1226, doi: 10.1126/science.aab0476.

Hennings, P. H., J. P. Nicot, R. S. Gao, H. R. DeShon, J. E. Lund Snee, A. P. Morris, M. R. Brudzinski, E. A. Horne, and C. Breton (2021). Pore pressure threshold and fault slip potential for induced earthquakes in the Dallas-Fort worth area of North Central Texas, *Geophys. Res. Lett.* **48,** e2021GL093564, doi: 10.1029/2021GL093564.

Hornbach, M. J., H. R. DeShon, W. L. Ellsworth, B. W. Stump, C. Hayward, C. Frohlich, H. R. Oldham, J. E. Olson, M. B. Magnani, C. Brokaw, *et al.* (2015). Causal factors for seismicity near Azle, Texas, *Nat. Comm.* **6,** 6728, doi: 10.1038/ncomms7728.

Horne, E. A., P. H. Hennings, J. L. Osmond, and H. R. DeShon (2020). Structural characterization of potentially seismogenic faults in the Fort Worth Basin, *Interpretation* **8,** T323–T347, doi: 10.1190/INT-2019-0188.1.

Huang, Y., L. De Barros, and F. Cappa (2019). Illuminating the rupturing of microseismic sources in an injection-induced earthquake experiment, *Geophys. Res. Lett.* **46,** 9563–9572, doi: 10.1029/2019GL083856.

Jeong, S. J., B. W. Stump, and H. R. DeShon (2020). Spectral characteristics of ground motion from induced earthquakes in the Fort Worth Basin, Texas using the generalized inversion technique, *Bull. Seismol. Soc. Am.* **110,** 2058–2076, doi: 10.1785/0120200097.

Jeong, S. J., B. W. Stump, H. R. DeShon, and L. Quinones (2021). Stress drop estimates for induced seismic events in the Fort Worth Basin, Texas, *Bull. Seismol. Soc. Am.* **111,** 1405–1421, doi: 10.1785/0120200268.

Justinic, A. H., B. W. Stump, C. Hayward, and C. Frohlich (2013). Analysis of the Cleburne, Texas, earthquake sequence from June 2009 to June 2010, *Bull. Seismol. Soc. Am.* **103,** 3083–3093, doi: 10.1785/0120120336.

Kanamori, H., and D. L. Anderson (1975). Theoretical basis of some empirical relations in seismology, *Bull. Seismol. Soc. Am.* **65,** 1073–1095, doi: 10.1785/BSSA0650051073.

Lengliné, O., L. Lamourette, L. Vivin, N. Cuenot, and J. Schmittbuhl (2014). Fluid-induced earthquakes with variable stress drop, *J. Geophys. Res.* **119,** 8900–8913, doi: 10.1002/2014JB011282.

Lund Snee, J. E., and M. D. Zoback (2016). State of stress in Texas: Implications for induced seismicity, *Geophys. Res. Lett.* **43,** 10,208–10,214, doi: 10.1002/2016GL070974.

Magnani, M. B., M. L. Blanpied, H. R. DeShon, and M. J. Hornbach (2017). Discriminating between natural versus induced seismicity from long-term deformation history of intraplate faults, *Sci. Adv.* **3,** e1701593, doi: 10.1126/sciadv.1701593.

Ogwari, P. O., H. R. DeShon, and M. J. Hornbach (2018). The Dallas-Fort Worth airport earthquake sequence: Seismicity beyond injection period, *J. Geophys. Res.* **123,** 553–563, doi: 10.1002/2017JB015003.

Quinones, L., H. R. DeShon, S. Jeong, P. Ogwari, O. Sufri, M. M. Holt, and K. B. Kwong (2019). Tracking induced seismicity in the Fort Worth Basin: A summary of the 2008–2018 North Texas earthquake study catalog, *Bull. Seismol. Soc. Am.* **109,** 1203–1216, doi: 10.1785/0120190057.

Quinones, L. A., H. R. DeShon, M. B. Magnani, and C. Frohlich (2018). Stress orientations in the Fort Worth Basin, Texas, determined from earthquake focal mechanisms, *Bull. Seismol. Soc. Am.* **108,** 1124–1132, doi: 10.1785/0120170337.

Reiter, D., M. Leidig, S. H. Yoo, and K. Mayeda (2012). Source characteristics of seismicity associated with underground wastewater disposal: A case study from the 2008 Dallas-Fort Worth earthquake sequence, *The Leading Edge* **31,** 1454–1460, doi: 10.1190/tle31121454.1.

Scales, M. M., H. R. DeShon, M. B. Magnani, J. I. Walter, L. Quinones, T. L. Pratt, and M. J. Hornbach (2017). A decade of induced slip on the causative fault of the 2015 M_W 4.0 Venus earthquake, northeast Johnson County, Texas, *J. Geophys. Res.* **122,** 7879–7894, doi: 10.1002/2017JB014460.

Staszek, M., B. Orlecka-Sikora, K. Leptokaropoulos, G. Kwiatek, and P. Martínez-Garzón (2017). Temporal static stress drop variations due to injection activity at The Geysers geothermal field, California, *Geophys. Res. Lett.* **44,** 7168–7176, doi: 10.1002/2017GL073929.

Sumy, D. F., C. J. Neighbors, E. S. Cochran, and K. M. Keranen (2017). Low stress drops observed for aftershocks of the 2011 M_W 5.7 Prague, Oklahoma, earthquake, *J. Geophys. Res.* **122,** 3813–3834, doi: 10.1002/2016JB013153.

Trugman, D. T., S. L. Dougherty, E. S. Cochran, and P. M. Shearer (2017). Source spectral properties of small to moderate earthquakes in southern Kansas, *J. Geophys. Res.* **122,** 8021–8034, doi: 10.1002/2017JB014649.

Wessel, P., W. H. Smith, R. Scharroo, J. F. Luis, and F. Wobbe (2013). Generic mapping tools: Improved version released, *Eos Trans. AGU* **94,** 409–410, doi: 10.1002/2013EO450001.

Yoshida, K., T. Saito, Y. Urata, Y. Asano, and A. Hasegawa (2017). Temporal changes in stress drop, frictional strength, and earthquake size distribution in the 2011 Yamagata-Fukushima, NE Japan, earthquake swarm, caused by fluid migration, *J. Geophys. Res.* **122,** 10,379–10,397, doi: 10.1002/2017JB014334.

Yu, H., R. M. Harrington, H. Kao, Y. Liu, R. E. Abercrombie, and B. Wang (2020). Well proximity governing stress drop variation and seismic attenuation associated with hydraulic fracturing induced earthquakes, *J. Geophys. Res.* **125,** e2020JB020103, doi: 10.1029/2020JB020103.

Zhai, G., and M. Shirzaei (2018). Fluid injection and time-dependent seismic hazard in the Barnett Shale, Texas, *Geophys. Res. Lett.* **45,** 4743–4753, doi: 10.1029/2018GL077696.

Manuscript received 4 February 2022
Published online 7 April 2022